DOI: 10.1002/ejic.200901163

Thermal Decomposition Reactions as a Tool for the Synthesis of New Thermodynamic Metastable Modifications: Synthesis, Structures, and Properties of (Formato)nickel(II) Coordination Polymers Based on 4,4′-Bipyridine

Jan Boeckmann,[a] Mario Wriedt,[a] and Christian Näther*[a]

Keywords: Coordination polymers / Transition metals / Crystal structures / Thermal properties / Magnetic properties / Solid-state structures

The reaction of nickel formate with 4,4′-bipyridine (bipy) in aqueous solution at room temperature leads to the formation of the hydrated compound $[Ni(HCO_2)_2(H_2O)(bipy)\cdot 4H_2O]_n$ (**1**) reported recently. On heating, compound **1** decomposes into the new anhydrous compound of composition $[Ni(HCO_2)_2(bipy)]_n$ (**2II**), which decomposes on further heating. Interestingly, if the anhydrous compound is prepared from solution, a new modification **2I** is obtained. Investigations on the stability of both forms show that modification **2I** presents the thermodynamically most stable form between room and decomposition temperature, whereas modification **2II**, which can only be prepared by thermal decomposition, is metastable. In the crystal structure of **2I**, the Ni^{2+} cations are coordinated by four μ_2-*anti,anti* bridging formato anions and two bridging μ_2-bipy ligands in a slightly distorted octahedral geometry. The formato anions bridge the metal cations in zigzag chains, which are further connected by μ_2-*anti,anti* formato anions and bipy ligands to give a three-dimensional coordination network. IR spectroscopic investigations on the metastable form **2II** also indicate that all formato anions act as bridging ligands. Magnetic measurements of the hydrated and anhydrous compounds reveal different behavior with a ferromagnetic ordering for compound **2I** and an antiferromagnetic ordering for compound **1**. For form **2II**, only Curie–Weiss paramagnetism was found.

Introduction

In recent years, enormous effort has been focused on the synthesis, structure determination, and elucidation of the properties of new coordination polymers and metal–organic frameworks.[1] The insertion of organic spacer ligands into coordination compounds resulted in a rich diversity and uncovered the pathway for the search for new functional materials with applications like energy storage, gasholder, catalysis, and photochemical or magnetic switchable materials.[2] In this context, it is of great interest to find correlations between the structure of the coordination compound and its properties to design specific structures with tunable characteristics for a wide range of applications. For the investigations of structure–property relationships, the phenomenon of polymorphism also has to be taken into account, which frequently occurs in solid-state chemistry because of the small differences in energies between the crystalline modifications.[3] Due to the fact that different polymorphic modifications often exhibit different chemical and physical properties, it is essential to include investigations on polymorphism.[4]

However, for the investigations of the properties of new coordination polymers, large and pure amounts of these compounds are required, which sometimes is difficult to achieve. In most cases the preparation of these compounds is carried out in solution, which leads to mixtures that have to be separated by hand. Therefore, alternative routes for the discovery and preparation of new phase-pure coordination polymers are needed.

Recently, we reported on ligand-rich (ligand-rich = rich in neutral coligands) coordination polymers of composition $[MX_2L_2]_n$ [X = NCS, L = pyrazine, pyrimidine, 4,4′-bipyridine (bipy)],[5,6] in which the small-sized thiocyanato anions are terminally N-bonded and therefore cannot be involved in magnetic exchange interactions. Investigations on their thermal behavior show that they decompose on heating into new ligand-deficient (ligand-deficient = lacking neutral coligands) compounds of composition $[MX_2L]_n$, in which the thiocyanato anions become μ-1,3-bridging and therefore can mediate magnetic exchange interactions. Consequently, depending on the nature of the organic spacer ligand and the metal involved, different magnetic properties were observed. It must be noted that the ligand-rich com-

[a] Institut für Anorganische Chemie, Universität zu Kiel, Max-Eyth-Straße 2, 24098 Kiel, Germany
Fax: +49-431-8801520
E-mail: cnaether@ac.uni-kiel.de

Supporting information for this article is available on the WWW under http://dx.doi.org/10.1002/ejic.200901163.

pounds can be prepared phase-pure in solution, whereas most of the ligand-deficient intermediates are obtained as mixtures but can be prepared phase-pure by thermal decomposition of their ligand-rich precursors. Thus, we have impressively shown that thermal decomposition reactions of suitable ligand-rich precursor compounds can be used as a convenient preparative tool for the facile synthesis of pure ligand-deficient coordination compounds in quantitative yield. In recent investigations we also have proven that a wide range of neutral coligands like alcohols or acetonitrile can be used for the preparation of the ligand-rich precursor compounds, and also the removal of coordinated water molecules from hydrated species, which will lead to denser structures and thus to different magnetic properties.[5,7]

On the basis of the above-mentioned investigations, we were interested to see if thermal decomposition reactions are limited to the preparation of new (thiocyanato)metal coordination polymers or can also be used for the synthesis of completely different compounds. Therefore, we have started systematic investigations in which a large amount of coordination polymers based on different transition metals and small-sized anions were examined. In this context, transition-metal formates are of interest because formato ligands might also enable cooperative magnetic phenomena.

In the beginning, the literature-known coordination polymers $[Ni(HCO_2)_2(H_2O)(bipy)\cdot 4H_2O]_n$ (**1**) and $[Co(HCO_2)_2(H_2O)(bipy)\cdot 4H_2O]_n$ (**3**) prepared in hydrothermal reactions were selected as model precursor compounds.[8] In their crystal structure the metal cations are coordinated by one terminal formato ligand, one water molecule, two μ_2-*anti*,*anti*-bridging formato ligands, and two N atoms of two bridging bipy ligands in a slightly distorted octahedral geometry (Figure 1, right). The formato ligands bridge the metal cations in zigzag chains, which are further connected by bipy ligands to give a three-dimensional coordination network. The open channels are filled with water molecules (Figure 1, left).

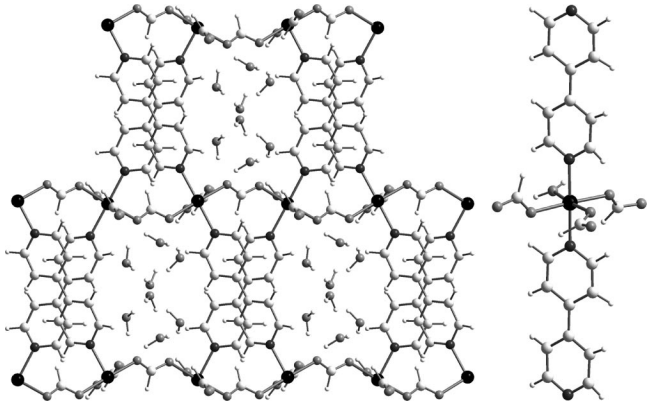

Figure 1. Crystal structure of **1** with a view along the crystallographic *c* axis (left) and its metal coordination sphere (right). Please note that the Co analogue **3** is isotypic.

A corresponding anhydrous phase of composition $[Co(HCO_2)_2(bipy)]_n$ (**4**)[8] was also reported but prepared in low yield at elevated temperature, whereas the analogous compound with nickel is unknown. Furthermore, the hydrated precursor compound **3** cannot be prepared phase-pure, and therefore only the Ni compound **1** was investigated.

Results and Discussion

Thermoanalytical Investigations

On heating of the hydrated compound **1** in a thermobalance to 400 °C, two mass steps were observed in the thermogravimetric (TG) curve that were accompanied by endothermic events in the differential thermal analysis (DTA) curve (Figure 2). From the derivative TG (DTG) curve, it is clear that the first steps are not well resolved, which can be explained by different kinds of water molecules in the crystal structure (channel and coordinated water). From the MS trend scan curve, it is proven that during the first mass steps only water (m/z = 18) is emitted, whereas during the second step carbon dioxide (m/z = 44) and bipy (m/z = 156) are emitted. The formation of carbon dioxide obviously originates from the pyrolysis of the formato ligands.

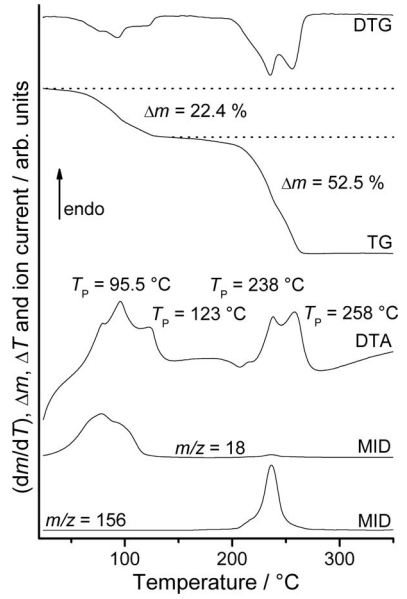

Figure 2. DTG, TG, DTA, and MS trend scan curves for **1**. Heating rate 4 °C min^{-1}; m/z = 18 (water), 156 (bipy); given are the mass changes [%] and the peak temperatures, T_P [°C].

The mass loss in the first step of $\Delta m_{exp.}$(1st step) = 22.4% is in reasonable agreement with that calculated for the loss of all water molecules [$\Delta m_{calcd.}$(–5H_2O) = 22.8%], whereas the mass loss in the second step of $\Delta m_{exp.}$(2nd step) = 52.5% corresponds roughly to the loss of carbon dioxide and bipy [$\Delta m_{calcd.}$(–carbon dioxide) + (–bipy) = 50.5%]. However, the theoretical mass loss for the second step is difficult to predict, because the overall reaction must be more complicated. However, on the basis of the experimental mass losses, it can be assumed that in the first heating step an anhydrous intermediate of composition $[Ni(HCO_2)_2$-

(bipy)]$_n$ is formed, whereas in the second step the removal of the bipy ligands and the decomposition of the metal formate occurs simultaneously. The residue obtained at 350 °C was identified as NiO by X-ray powder diffraction (XRPD) investigations.

To verify the nature of the intermediate formed, additional TG measurements were performed and stopped after the first TG step. Elemental analysis of the residue obtained yielded a composition of [Ni(HCO$_2$)$_2$(bipy)]$_n$ (**2II**) (see the Experimental Section). Interestingly, XRPD investigations of compound **2II** proved that it is not isotypic to the corresponding anhydrous compound [Co(HCO$_2$)$_2$-(bipy)]$_n$ (**4**)[8] reported recently (Figure 3).

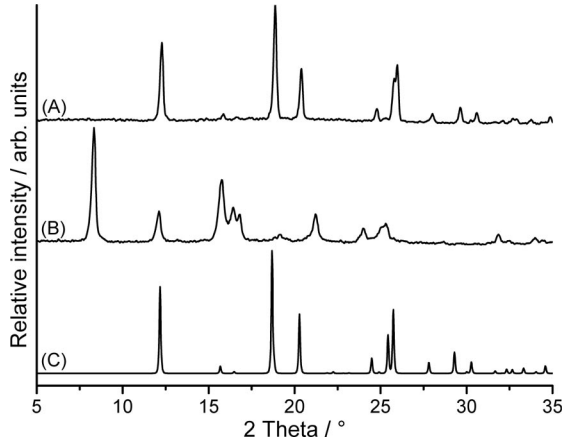

Figure 3. Experimental XRPD pattern of **2I** (A), **2II** (obtained in the first TG step in the thermal decomposition reaction of **1**) (B), and the XRPD pattern calculated from single-crystal data for **4** (C).[8]

To determine the crystal structure of the anhydrous compound, single crystals were prepared under solvothermal conditions. Surprisingly, we obtained crystals of the anhydrous phase from solution that are isotypic to its Co analogues, and therefore different polymorphic modifications were obtained in solution (form **2I**) and by dehydration (form **2II**). However, single crystals of form **2II** cannot be prepared in solution, and all attempts to determine the structure of **2II** on the basis of X-ray powder data were not successful (see the Experimental Section).

Crystal Structure

Form **2I** of [Ni(HCO$_2$)$_2$(bipy)]$_n$ crystallizes in the noncentrosymmetric tetragonal space group $P4_32_12$ with four formula units in the unit cell and is isotypic to the Co, Cu, Mn, and Zn compounds reported recently.[8,9] The asymmetric unit consists of one Ni^{2+} cation located on a twofold rotation axis as well as of one formato ligand and of one bipy ligand on a twofold rotation axis. In the crystal structure, the metal cations are coordinated by four O atoms of four formato ligands and two N atoms of two bridging bipy ligands in a slightly distorted octahedral geometry (Figure 4). The formato ligands bridge the metal cations in zigzag chains, which are further connected by μ_2-*anti*,*anti* formato ligands to give a three-dimensional coordination network (Figure 5). From this arrangement, channels are formed that elongate in the direction of the *a* and *b* axes. The bipy ligands are located in the channels and connect opposite Ni cations.

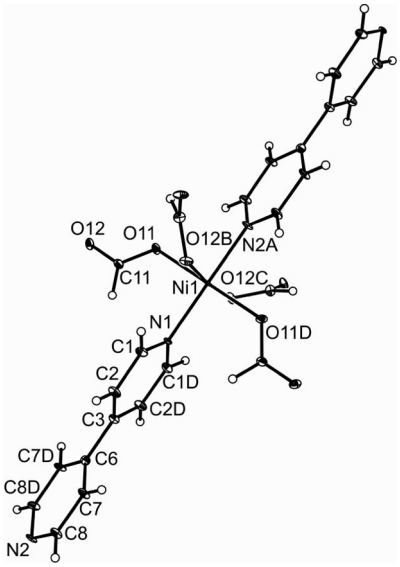

Figure 4. Crystal structure of [Ni(HCO$_2$)$_2$(bipy)]$_n$ (**2I**) with view of the coordination sphere of the metal cation with labeling and displacement ellipsoids drawn at the 50% probability level. Symmetry codes: A: $x + 1$, $y + 1$, z; B: $x + ½$, $–y + ½$, $–z + ¼$; C: $–y + ½$, $x + ½$, $z – ¼$; D: y, x, $–z$.

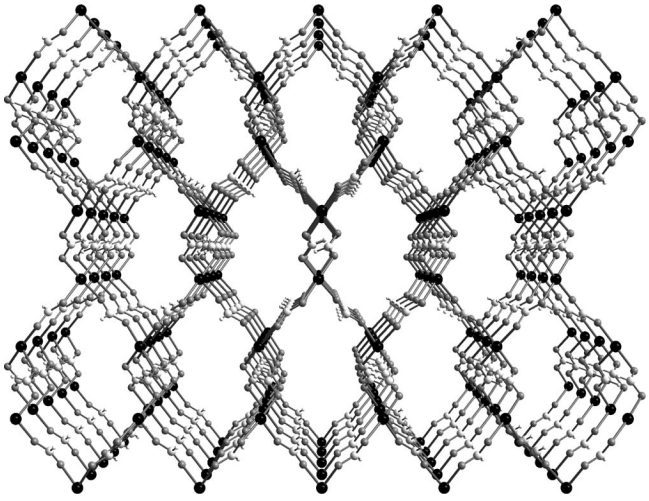

Figure 5. Crystal structure of **2I** with a view along the crystallographic *b* axis. The bipy ligands are omitted for clarity.

The Ni–N and Ni–O distances range between 2.072(2) and 2.1329(16) Å, and the angles around the Ni^{2+} cation range between 87.24(5) and 92.76(5)° (Table 1). The intranetwork metal–metal separation through the bipy ligand amounts to 11.2004(5) Å, and the metal–metal separation through the formato ligands amounts to 5.8892(3) Å. The latter vary in the literature from 3.0860 Å[10] to 6.0120 Å.[11] The dihedral angle between six-membered rings of the bipy ligands amount to 47.03(1)°. All distances and angles are

comparable to those found in its Co, Cu, Mn, and Zn analogues with slight differences due to the different ionic radii of the metal cations.

Table 1. Selected bond lengths [Å] and angles [°] for **2I**.

Ni1–N1	2.072(2)
Ni1–N2A	2.075(2)
Ni1–O11	2.1329(16)
Ni1–O12B	2.1267(15)
N1–Ni1–N2A	180.00(6)
N1–Ni1–O12B	92.76(5)
N1–Ni1–O11	90.07(5)
N2A–Ni1–O12B	87.24(5)
N2A–Ni1–O11	89.93(5)
O11–Ni1–O11D	179.85(10)
C1–N1–Ni1	120.64(13)

Thermodynamic Stability

To verify which of the two polymorphic modifications **2I** and **2II** represents the thermodynamically most stable form at room temperature, the stability of both forms was investigated by solvent-mediated conversion experiments. In this experiment, equivalent amounts of both forms were stirred in a saturated solution of dmf, which contained an excess amount of both crystalline forms, and the precipitates were investigated by XRPD (Figure 6). These experiments clearly showed that after 1 week only modification **2I** was present, which proves that this modification represents the thermodynamic most stable form at room temperature, whereas the intermediate **2II** prepared by dehydration is metastable (Figure 6).

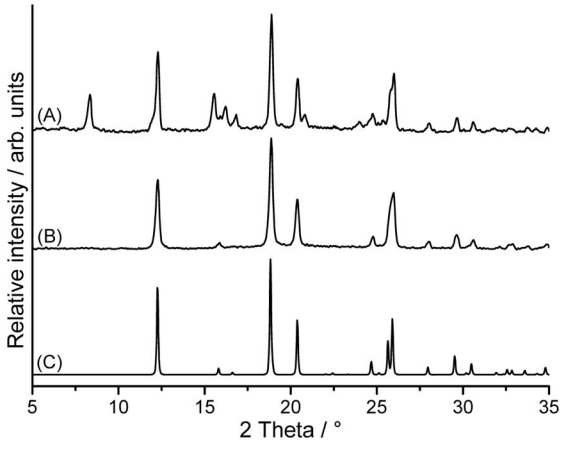

Figure 6. Experimental XRPD patterns of a mixture of the polymorphic **2I** and **2II** before (A) and after (B) stirring for 1 week in dmf, together with the calculated XRPD pattern from single-crystal data for **2I** (C).

From the DTA curve presented in Figure 2, there is no hint of a polymorphic phase transition. Therefore, investigations using differential scanning calorimetry (DSC) were performed. On heating form **2II**, a very weak and broad endothermic signal was observed at about 84 °C, followed by a weak exothermic transition at 190 °C. On further heating, decomposition was observed at a peak temperature of 252 °C (Figure 7). Additional DSC measurements always showed a similar thermal behavior. From these measurements, there is evidence of a transformation of form **2II** before decomposition.

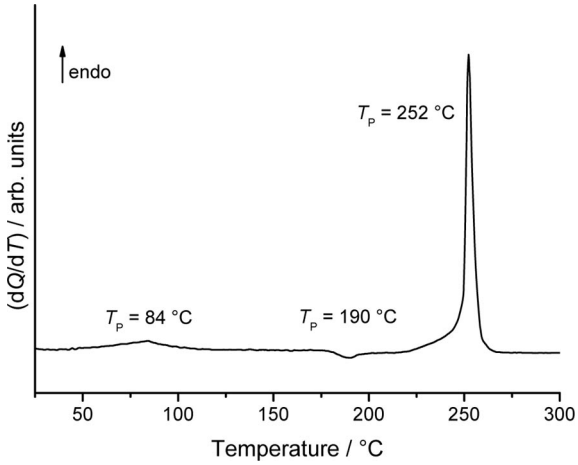

Figure 7. DSC curve of **2II**. Heating rate 3 °C min^{-1}; Al pans; peak temperatures, T_P [°C], are given.

To verify the nature of the intermediates formed, additional DSC measurements were performed. When the reaction was stopped after the exothermic peak at about 210 °C and the residue was investigated by XRPD investigations, it was proven that a polymorphic transformation into form **2I** occurred (Figure 8). When the residue formed in the first endothermic transition was investigated by XRPD measurements, only a few changes in the diffraction pattern were observed. This might indicate the formation of a further modification of compound **2**. However, from this experiment it is clear that form **2I** is more stable at higher temperatures. As this modification also represents the most stable form at room temperature, it can be assumed that forms **2I** and **2II** should behave monotropically between room and decomposition temperature.

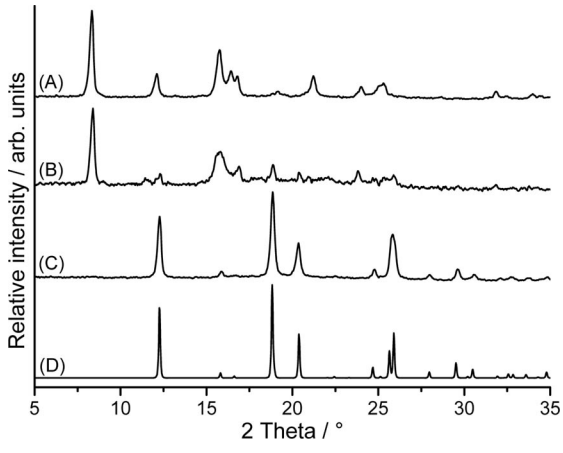

Figure 8. Experimental XRPD patterns of **2II** (A), and the residues isolated at 110 °C (B) and 210 °C (C) together with the calculated XRPD pattern for **2I** (D).

Investigations on the Reversibility of the Removal of the Water Molecules

To investigate the reversibility of the dehydration of form **1**, the metastable form **2II**, obtained after the first TG step, was prepared on an XRPD sample holder and left undisturbed under ambient atmosphere. Afterwards XRPD investigations were performed every 24 h. These investigations showed clearly that within 72 h full reversibility is achieved (Figure 9).

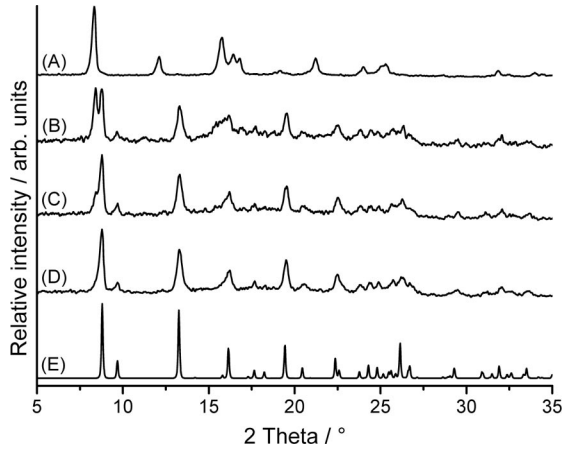

Figure 9. Experimental XRPD patterns of the residue obtained in a rehydration experiment of **2II** after 0 h (A), 24 h (B), 48 h (C), and 72 h (D), as well as a calculated XRPD pattern from single-crystal data for **1** (E).

Similar investigations on the most stable form **2I** showed no rehydration within several days. Thus, defined amounts of **2I** were stirred in water at room temperature, and the resulting precipitate was investigated by ex-situ time-dependent XRPD measurements (Figure 10). These experiments clearly showed that even within 1 month not all of the material had transformed into compound **1**, which indicates a high stability of the thermodynamic most stable form **2I** (compare A with B in Figure 10). It must be noted

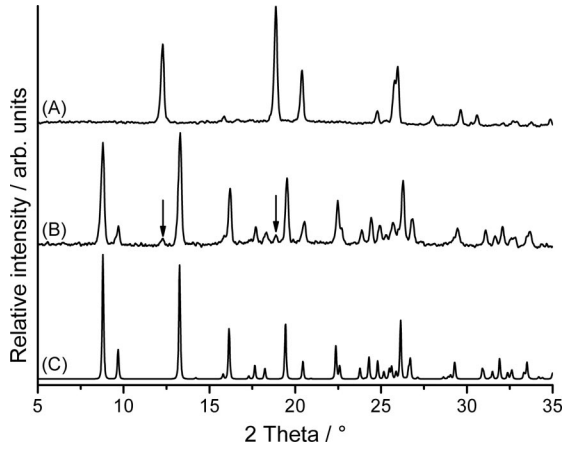

Figure 10. Experimental XRPD patterns of the thermodynamic stable **2I** (A) and of the residue formed in a rehydration experiment after 1 month (B) together with the calculated XRPD pattern from single-crystal data for **1** (C).

that the hydration and rehydration is accompanied by a change of color (compounds **2I** and **2II**: green; compound **1**: blue).

Infrared Spectroscopic Investigations

For the metastable form **2II**, no single crystals can be obtained, and therefore no structural information is accessible. Thus, the different bridging modes of the formato ligands were investigated by IR spectroscopy.

To verify the bridging modes of formato ligands it is important to determine the difference of the wavenumber values between the very strong asymmetric (ν_{as}) and the weaker symmetric (ν_s) C–O valence vibration ($\Delta\nu = \nu_s - \nu_{as}$).[12,13] Earlier investigations showed clearly that a $\Delta\nu$ value much larger than about 250 cm^{-1} indicates terminal-coordinated formate groups, like in $[Ph_4Sb(O_2CH)]$ ($\Delta\nu$ = 350 cm^{-1}),[13] whereas $\Delta\nu$ values below this value are significant for compounds with bridging formate groups like in $Cu(O_2CH)_2{\cdot}2H_2O$ (*anti*,*anti*-bridged: $\Delta\nu$ = 196 cm^{-1}) and $[Cu(O_2CH)_2\{CO(NH_2)_2\}]$ (*syn*,*syn*-bridged: $\Delta\nu$ = 238 cm^{-1}).[13] For compound **2I**, we identified the asymmetric C–O valence vibration at 1563 cm^{-1} and the symmetric C–O valence vibration at 1349 cm^{-1} (see Figure S2 in the Supporting Information). The resulting $\Delta\nu$ value of 214 cm^{-1} is in agreement with *anti*,*anti*-bridging formato ligands in this compound (see the section on Crystal Structure above). In compound **1**, terminal and *anti*,*anti*-bridged formato ligands are present. Therefore, a splitting of the asymmetric and the symmetric C–O valence vibration and two different $\Delta\nu$ values are observed (see Figure S1 in the Supporting Information). The value $\Delta\nu$ = 224 cm^{-1} must correspond to bridging and that of $\Delta\nu$ = 270 cm^{-1} to the terminally bonded formato ligands.

In the IR spectrum of the metastable form **2II**, no splitting is observed. Also, the asymmetric C–O valence vibration is observed at 1586 cm^{-1} and the symmetric C–O valence vibration at 1362 cm^{-1}, thereby leading to a $\Delta\nu$ value of 224 cm^{-1}. This clearly indicates that only bridging formato ligands are present (see Figure S3 in the Supporting Information). Therefore, it can be concluded that the water molecules coordinated to the Ni^{2+} centers are replaced by the terminally bonded formato ligands.

Magnetic Investigations

In compounds **1**, **2I**, and **2II**, the metal centers are separated by only 3 atoms of the formato ligands, which might enable cooperative magnetic phenomena. To investigate their magnetic properties, the temperature dependence of their susceptibilities was investigated by applying a magnetic field of H = 0.1 T in the temperature range of 300–2 K (Figures 11, 12, and 13). For compound **2I**, the χ_M versus T curve shows ferromagnetic behavior (Figure 11A). Fitting of the magnetic data according to the Curie–Weiss law $\chi_M = C/(T - \theta)$ yields a positive Weiss constant of θ = 17.39 K and a Curie constant of C = 1.76 $cm^3\,K\,mol^{-1}$ (Table 2), thereby indicating net ferromagnetic interactions between

the Ni^{2+} centers. In the temperature range of 300–25 K, the $\chi_M T$ values decrease upon cooling, thus indicating antiferromagnetic interactions, and below 25 K the curve passes a sharp maximum at T_C = 21.2 K, thereby suggesting a transition to the ferromagnetic state (Figure 11A). Below the maximum, the $\chi_M T$ values decrease again upon cooling, which means that below T_C antiferromagnetic interactions seem to dominate (Figure 11A). The experimental effective magnetic moment (μ_{eff}) of 3.78 μ_B is higher than the spin-only value of 2.83 μ_B for a high-spin Ni^{2+} ion (S = 1, g = 2.0), but due to the orbital contribution from single octahedral Ni^{2+} ions it is not unusual[14] (Table 2). Furthermore, the field-cooled (FC) magnetization curve (H = 0.1 T) exhibits a steep increase at around T_C = 21.2 K (Figure 11B).

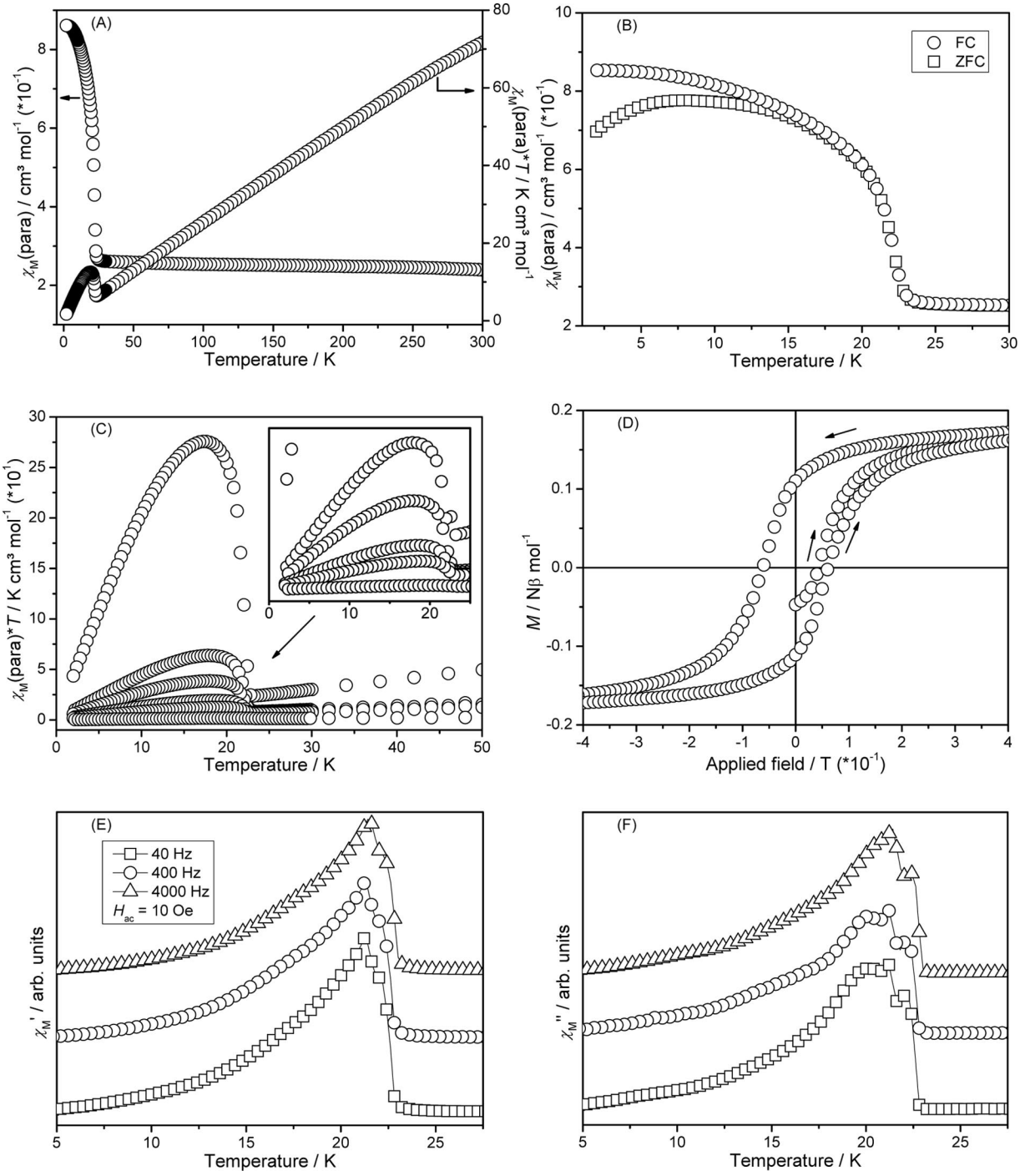

Figure 11. Results of the magnetic measurements for **2I** by plots of paramagnetic susceptibility and $\chi_M T$ as function of temperature (A), ZFC (at H = 0.1 T) and FC (at H = 0.1 T) paramagnetic susceptibility as function of temperature (B), field-dependent $\chi_M T$ as function of temperature (H = 20/100/200/500/1000, and 10000 Oe from top to bottom in the plot) (C), hysteresis loop of a ±4 T range at T = 4 K (D), temperature dependence of in-phase χ_M' (E) and out-of-phase χ_M'' (F) alternating-current (ac) magnetic susceptibility (H_{ac} = 10 Oe; 40/400/4000 Hz).

The difference between FC and zero-field-cooled (ZFC) curves below the transition temperature is another hint of ferromagnetic long-range order. Note that FC and ZFC curves match perfectly above T_C (Figure 11B). The $\chi_M T$ values are field-dependent, especially below the critical temperature of 21.2 K (Figure 11C). Under external fields of 20, 100, 200, 500, 1000, and 10000 Oe, the maximum in the $\chi_M T$ versus T curve ranges from 1.86 to 275.64 K cm^3 mol^{-1} (Figure 11C).

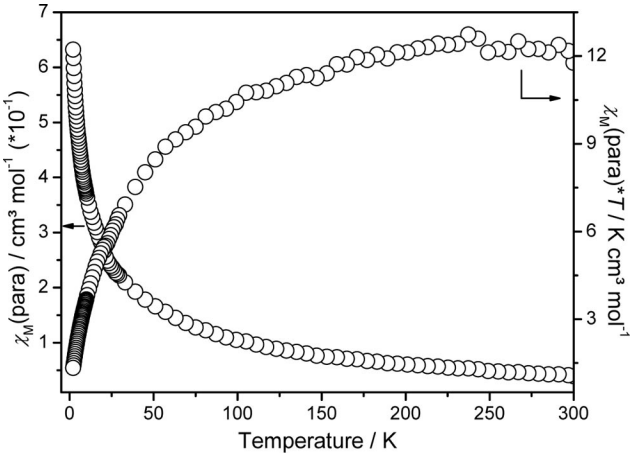

Figure 12. Results of the magnetic measurements by plots of paramagnetic susceptibility and $\chi_M T$ as function of temperature for intermediate $[Ni(HCO_2)_2(bipy)]_n$ (**2II**).

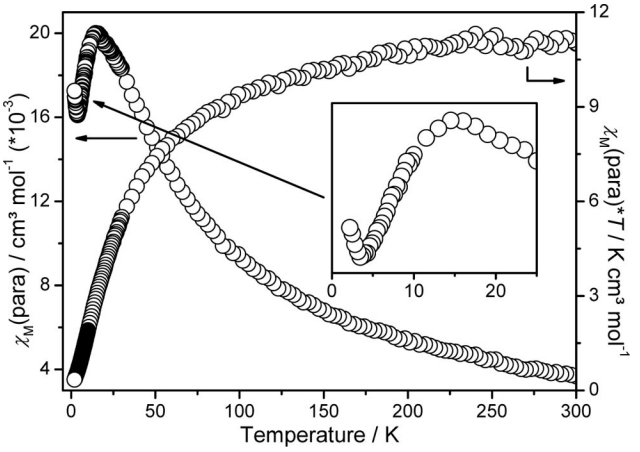

Figure 13. Results of the magnetic measurements by plots of paramagnetic susceptibility and $\chi_M T$ as function of temperature for $[Ni(HCO_2)_2(H_2O)(bipy)\cdot 4H_2O]_n$ (**2**).

Further hints of the presence of ferromagnetic properties are provided by the magnetization saturation experiments performed at T = 4 K up to 4 T (Figure 11D). Herein the occurrence of a hysteresis loop (Figure 11D) is typical for ferromagnetic properties, and the relatively low value for the coercive field of H_c = 0.06 T and a remanent magnetization of M_r = 0.11 Nβ mol^{-1} suggests soft ferromagnetic behavior. Further evidence for the ferromagnetic properties is supplied by alternating-current susceptibility measurements (Figure 11E and F). Both the χ_M' and χ_M'' (in-phase and out-of-phase) curves exhibit a sharp maximum at the transition temperature of 21.2 K (Figure 11E and F), a typical behavior of ferromagnetic materials. The shoulders in the χ_M'' curve near the maximum are caused by relaxation and dissipation processes within the material. It must be pointed out that there is no disarrangement of the peak maxima.

Table 2. Results of the fits of the magnetic susceptibility data with the Curie–Weiss law for **1**, **2I**, and **2II**.

	1[a]	**2I**	**2II**
C [cm^3 K mol^{-1}]	1.27	1.76	1.43
θ [K]	–36.78	17.39	–35.98
μ_{eff} (exp.) [μ_B]	3.19	3.76	3.39
μ_{eff} (calcd.)[14] [μ_B]	2.83	2.83	2.83
Ordering state [K]	T_N = 14.5	T_C = 21.2	–
Fit [K]	33–231	19–24	25–231

[a] This work.

For the anhydrous metastable intermediate **2II**, only Curie–Weiss paramagnetism is found (Figure 12). Only the negative Weiss constant θ = –35.98 K, a Curie constant of C = 1.43 cm^3 K mol^{-1} (Table 2), and the decrease of the $\chi_M T$ values upon cooling (Figure 12) indicate weak antiferromagnetic interactions between the nickel(II) centers. The effective magnetic moment μ_{eff} of 3.39 μ_B for **2II** is higher than the spin-only value of 2.83 μ_B for a high-spin Ni^{2+} ion (S = 1, g = 2.0) (Table 2).

Compound **1** was already investigated by the group of Wang et al.,[8] but for purposes of comparison this compound was investigated in addition. The overall data are in good agreement with that reported, and only small differences are found in the Weiss constant (θ = –29.9 K), in the Néel temperature (T_N = 17 K), and in the Curie constant (C = 1.30 cm^3 K mol^{-1}). Our measurements reveal that for compound **1** a sharp maximum in the χ_M versus T curve is observed, which indicates an antiferromagnetic ordering at T_N = 14.5 K (Figure 13). Above this ordering temperature, the χ_M^{-1} versus T curve is essentially linear and follows the Curie–Weiss law. The negative Weiss constant of θ = –36.78 K (Table 2) and the decrease of the $\chi_M T$ versus T curve upon cooling (Figure 13) confirm the antiferromagnetic behavior. The effective magnetic moment μ_{eff} of 3.19 μ_B for **1** is in rough agreement with the spin-only value of 2.83 μ_B for a high-spin Ni^{2+} ion (S = 1, g = 2.0) (Table 2).

Conclusion

The hydrated compound $[Ni(HCO_2)_2(H_2O)(bipy)\cdot 4H_2O]_n$ (**1**) was investigated for its thermal properties. On heating, a two-step decomposition was observed, in which the first step is related to the phase-pure formation of a new anhydrous intermediate (**2II**), which on further heating transforms into a second modification (**2I**), which decomposes in the second step. Solvent-mediated conversion experiments and DSC measurements clearly showed that form **2I** represents the thermodynamically most stable form, whereas form **2II** is metastable. The thermodynamically most stable modification **2I** can also be obtained by solvothermal reactions, whereas the metastable modification **2II**

is only accessible by water removal of its hydrated precursor compound **1**. In the crystal structure of the hydrated precursor compound **1**, the metal cations are coordinated to one terminal formato ligand and one water molecule and are μ_2-*anti*,*anti*-bridged by two formato ligands and two N atoms of two bridging bipy ligands, whereas in the anhydrous compound **2I** all formato ligands are bridging. IR investigations indicate that even in form **2II** only bridging anions are found. Interestingly, in the stable form **2I** a ferromagnetic transition is observed, whereas in the metastable form **2II** only Curie–Weiss behavior is found. This indicates that different connection modes are present in both forms, which cannot be clearly identified only on the basis of our spectroscopic investigations.

We have shown that the removal of coligands by thermal decomposition is an alternative tool for the discovery and preparation of new phases including polymorphic modifications in quantitative yield, which very often cannot be prepared in solution. One advantage of this method is that the reaction must lead to compounds with a higher degree of condensation, and therefore different magnetic properties are observed.

For a better understanding of the magneto-structural correlations, much more systematic investigations are needed. Thus, similar formato compounds based on other N-donor ligands like pyrazine, pyrimidine, pyridazine, and 4,4′-bipyridine will be investigated in the future.

Experimental Section

Synthesis: $Ni(HCO_2)_2{\cdot}2H_2O$ and bipy were obtained from Alfa Aesar. Solvents were used without further purification. Crystalline powders of compound **1** and **2I** were prepared by stirring the reactants in appropriate solvents at room or elevated temperature. The residues were filtered off and washed with ethanol and diethyl ether and dried in air. Compound **2II** can only be prepared by thermal decomposition of compound **1**. The purity of all compounds was checked by X-ray powder diffraction and elemental analysis.

Synthesis of Poly[aqua(μ_2-4,4′-bipyridine-*N*,*N*′)(μ_2-formato-*O*,*O*′)-(formato-*O*)nickel(II)·4H$_2$O] (1): The literature-known compound **1** was prepared according to a different procedure with higher yield by the reaction of $Ni(HCO_2)_2{\cdot}2H_2O$ (46.2 mg, 0.25 mmol) and bipy (39.9 mg, 0.25 mmol) in water (3.00 mL). Yield: 69.4 mg (91%). $C_{12}H_{20}N_2NiO_9$ (395.0): calcd. C 36.49, H 5.10, N 7.09; found C 36.89, H 5.34, N 7.37. IR (KBr): $\tilde{\nu}$ = 3330 (b), 2884 (w), 2842 (w), 1610 (s), 1590 (s), 1539 (m), 1493 (w), 1415 (m), 1393 (m), 1385 (m), 1366 (m), 1341 (m), 1224 (m), 1072 (m), 827 (m), 810 (w), 733 (w), 636 (m) cm^{-1}.

Synthesis of Poly[(μ_2-4,4′-bipyridine-*N*,*N*′)(μ_2-formato-*O*,*O*′)nickel-(II)] (2I): A green crystalline powder was prepared by the reaction of $Ni(HCO_2)_2{\cdot}2H_2O$ (46.2 mg, 0.25 mmol) and 4,4′-bipy (39.9 mg, 0.25 mmol) in dmf (3.00 mL) and heating to 130 °C for 4 d. Yield: 67.6 mg (89%). Green well-shaped single crystals suitable for X-ray structure determination were obtained by slow concentration of the filtrate. $C_{12}H_{10}N_2NiO_4$ (304.9): calcd. C 47.27, H 3.31, N 9.19; found C 47.67, H 3.29, N 9.57. IR (KBr): $\tilde{\nu}$ = 3058 (w), 3039 (w), 3019 (w), 2864 (w), 1614 (m), 1563 (s), 1537 (s), 1490 (m), 1396 (m), 1388 (m), 1349 (m), 1223 (w), 835 (m), 783 (m), 640 (w), 531 (w) cm^{-1}.

Elemental Analysis and Spectroscopic Investigation of the Residue Obtained in the Thermal Decomposition: Isolated in the first heating step (see the Thermoanalytic Investigations section in the Results and Discussion) of compound **1**. Calculated for the ligand-deficient compound **2II**. $C_{12}H_{10}N_2NiO_4$ (304.9): C 47.27, H 3.31, N 9.19; found C 47.58, H 3.52, N 9.56. IR (KBr): $\tilde{\nu}$ = 3075 (w), 2850 (w), 1586 (s), 1534 (m), 1488 (m), 1411 (m), 1362 (s), 1318 (w), 1219 (m), 1067 (m), 813 (m), 733 (w), 633 (m) cm^{-1}.

Single-Crystal Structure Analysis: Data measurement was performed with an imaging-plate diffraction system (IPDS-1) with Mo-K_α radiation from STOE & CIE. The structure solution was carried out with direct methods by using SHELXS-97, and structure refinements were performed against F^2 by using SHELXL-97.[15] All non-hydrogen atoms were refined with anisotropic displacement parameters. All hydrogen atoms were positioned with idealized geometry and were refined with fixed isotropic displacement parameters [U_{eq}(H) = –1.2U_{eq}(C) (–1.5 for methyl H atoms)] by using a riding model with $d_{C–H}$ = 0.95 Å for aromatic and $d_{C–H}$ = 1.00 Å for aliphatic H atoms. Details of the structure determination are given in Table 3. CCDC-765671 (**2I**) contains the supplementary crystallographic data for this paper. These data can be obtained free of charge from The Cambridge Crystallographic Data Centre via www.ccdc.cam.ac.uk/data_request/cif.

Table 3. Selected crystal data and details of the structure determinations from single-crystal data for **2I**.

Empirical formula	$C_{12}H_{10}N_2NiO_4$
M_r [g mol^{-1}]	304.93
Crystal system	tetragonal
Space group	$P4_32_12$
a [Å]	7.9199(3)
c [Å]	17.4127(9)
V [Å^3]	1092.21(8)
T [K]	170
Z	4
$D_{calcd.}$ [g cm^{-3}]	1.854
μ [mm^{-1}]	1.788
$\theta_{max.}$ [°]	27.98
Measured reflections	8556
Unique reflections	1321
Reflections [$F_o > 4\sigma(F_o)$]	1210
Parameters	90
R_{int}	0.0600
R_1[a] [$F_o > 4\sigma(F_o)$]	0.0267
wR_2[b] (all data)	0.0638
GOF	1.052
$\Delta\rho_{max.}$, $\Delta\rho_{min.}$ [e Å^{-3}]	0.439, –0.437

[a] $R_1 = \Sigma||F_o| - |F_c||/\Sigma|F_o|$. [b] $wR_2 = \{\Sigma[w(F_o^2 - F_c^2)^2]/\Sigma[w(F_o^2)^2]\}^{1/2}$.

X-ray Powder Diffraction (XRPD): XRPD experiments were performed by using a Stoe Transmission Powder Diffraction System (STADI P) with Cu-K_α radiation (λ = 154.0598 pm) that was equipped with a linear position-sensitive detector (scan range = 2–130°) from STOE & CIE. To retrieve additional structural information on the metastable modification **2II**, we tried to index the powder pattern of this form but did not find any reasonable unit cell. The difficulties may arise from the extremely strong reflection broadening caused by the thermal dehydration process.

Differential Thermal Analysis, Thermogravimetry, and Mass Spectroscopy (DTA-TG-MS): The DTA-TG measurements were performed under nitrogen (purity: 5.0) in Al_2O_3 crucibles with an STA-409CD instrument from Netzsch. The DTA-TG-MS measurements were performed with the same instrument, which was con-

nected to a quadrupole mass spectrometer from Balzers through Skimmer coupling from Netzsch. The MS measurements were performed in analogue and trend-scan mode in Al_2O_3 crucibles in a dynamic helium environment (purity: 5.0) by using heating rates of 4 °C min^{-1}. All measurements were performed with a flow rate of 75 mL min^{-1} and were corrected for buoyancy and current effects. The instrument was calibrated by using standard reference materials.

Differential Scanning Calorimetry: DSC experiments were performed with the DSC 204/1/F from Netzsch in alumina crucibles. For all compounds, several measurements were performed by using heating rates of 3 and 10 °C min^{-1}. The calorimeter was calibrated by using standard reference substances. All characteristic temperatures were estimated from different measurements at 3 °C min^{-1}.

Elemental Analysis: CHNS analyses were performed with a EURO EA elemental analyzer, fabricated by EURO VECTOR Instruments and Software.

Spectroscopy: Fourier transform IR spectra were recorded in KBr pellets with a Genesis series FTIR spectrometer by ATI Mattson.

Magnetic Measurements: Magnetic measurements were performed with a physical property measuring system (PPMS) from Quantum Design, which was equipped with a 9 T magnet. The data were corrected for core diamagnetism.[16]

Supporting Information (see footnote on the first page of this article): Experimental and calculated X-ray powder pattern for compounds **1** and **2I**, IR spectra of compounds **1**, **2I**, and **2II**, and a DTA-TG curve of compound **2I**.

Acknowledgments

We gratefully acknowledge financial support by the State of Schleswig-Holstein, and we thank Professor Dr. Wolfgang Bensch for the opportunity to use his experimental facility. Special thanks go to Inke Jeß for her support in single-crystal measurements.

[1] A. J. Blake, N. R. Champness, P. Hubberstey, W.-S. Li, M. A. Withersby, M. Schröder, *Coord. Chem. Rev.* **1999**, *183*, 117–138; C. Janiak, L. Uehlin, H.-P. Wu, P. Klüfers, H. Piotrowski, T. G. Scharmann, *J. Chem. Soc., Dalton Trans.* **1999**, 3121–3131; A. J. Blake, N. R. Brooks, N. R. Champness, M. Crew, D. H. Gregory, P. Hubberstey, M. Schröder, A. Deveson, D. Fenske, L. R. Hanton, *Chem. Commun.* **2001**, 1432–1433; A. N. Khlobystov, A. J. Blake, N. R. Champness, D. A. Lemenovskii, A. G. Majouga, N. V. Zyk, M. Schröder, *Coord. Chem. Rev.* **2001**, *222*, 155–192; B. Moulton, M. J. Zaworotko, *Chem. Rev.* **2001**, *101*, 1629–1658; R. J. Puddephatt, *Coord. Chem. Rev.* **2001**, *216–217*, 313–332; S. R. Batten, K. S. Murray, *Coord. Chem. Rev.* **2003**, *246*, 103–130; S. L. James, *Chem. Soc. Rev.* **2003**, *32*, 276–288; C. Janiak, *Dalton Trans.* **2003**, 2781–2804; D. Maspoch, D. Ruiz-Molina, J. Veciana, *J. Mater. Chem.* **2004**, *14*, 2713–2723; S. Kitagawa, K. Uemura, *Chem. Soc. Rev.* **2005**, *34*, 109–119; A. Y. Robin, K. M. Fromm, *Coord. Chem. Rev.* **2006**, *250*, 2127–2157; S. Kitagawa, R. Matsuda, *Coord. Chem. Rev.* **2007**, *251*, 2490–2509; D. Maspoch, D. Ruiz-Molina, J. Veciana, *Chem. Soc. Rev.* **2007**, *36*, 770–818.

[2] G. Férey, *Dalton Trans.* **2009**, 4400–4415; M. Xue, G. S. Zhu, Y. X. Li, X. J. Zhao, Z. Jin, E. Kang, S. L. Qiu, *Cryst. Growth Des.* **2008**, *8*, 2478–2483; M. Eddaoudi, J. Kim, N. Rosi, D. Vodak, J. Wachter, M. O'Keeffe, O. M. Yaghi, *Science* **2002**, *295*, 469–472; S. Hu, L. Yun, Y. Z. Zheng, Y. H. Lan, A. K. Powell, M. L. Tong, *Dalton Trans.* **2009**, 1897–1900; X.-Y. Wang, Z.-M. Wang, S. Gao, *Chem. Commun.* **2007**, 1127–1129; M. L. Liu, W. Shi, H. B. Song, P. Cheng, D. Z. Liao, S. P. Yan, *CrystEngComm* **2009**, *11*, 102–108; W. X. Zhang, W. Xue, J. B. Lin, Y. Z. Zheng, X. M. Chen, *CrystEngComm* **2008**, *10*, 1770–1776; X.-Y. Wang, Z.-M. Wang, S. Gao, *Chem. Commun.* **2008**, 281–294; E. Pardo, R. Ruiz-Garcia, J. Cano, X. Ottenwaelder, R. Lescouezec, Y. Journaux, F. Lloret, M. Julve, *Dalton Trans.* **2008**, 2780–2805; W. Li, H.-P. Jia, Z.-F. Ju, J. Zhang, *Dalton Trans.* **2008**, 5350–5357; H. A. Habib, J. Sanchiz, C. Janiak, *Dalton Trans.* **2008**, 4877–4884; H. A. Habib, J. Sanchiz, C. Janiak, *Dalton Trans.* **2008**, 1734–1744; K. S. Gavrilenko, O. Cador, K. Bernot, P. Rosa, R. Sessoli, S. Golhen, V. V. Pavlishchuk, L. Ouahab, *Chem. Eur. J.* **2008**, *14*, 2034–2043; K. Drabent, Z. Ciunik, A. Ozarowski, *Inorg. Chem.* **2008**, *47*, 3358–3365; M. A. M. Abu-Youssef, A. Escuer, F. A. Mautner, L. Ohrstrom, *Dalton Trans.* **2008**, 3553–3558; A. Prescimone, J. Wolowska, G. Rajaraman, S. Parsons, W. Wernsdorfer, M. Murugesu, G. Christou, S. Piligkos, E. J. L. McInnes, E. K. Brechin, *Dalton Trans.* **2007**, 5282–5289; H. Miyasaka, M. Yamashita, *Dalton Trans.* **2007**, 399–406; L. M. Toma, R. Lescouezec, J. Pasan, C. Ruiz-Perez, J. Vaissermann, J. Cano, R. Carrasco, W. Wernsdorfer, F. Lloret, M. Julve, *J. Am. Chem. Soc.* **2006**, *128*, 4842–4853; M. Verdaguer, A. Bleuzen, C. Train, R. Garde, F. F. d. Biani, C. Desplanches, *Phil. Trans. R. Soc. A* **1999**, *357*, 2959–2976; A. J. Epstein, J. S. Miller, *Angew. Chem.* **1994**, *106*, 399–432; *Angew. Chem. Int. Ed. Engl.* **1994**, 385–415.

[3] S. R. Batten, K. S. Murray, *Aust. J. Chem.* **2001**, *54*, 605–609; J. Bernstein, *J. Phys. D: Appl. Phys.* **1993**, *26*, B66–B76; J. Bernstein, R. J. Davey, J.-O. Henck, *Angew. Chem.* **1999**, *111*, 3646–3669; *Angew. Chem. Int. Ed.* **1999**, *38*, 3440–3461.

[4] M. Wriedt, C. Näther, *Z. Anorg. Allg. Chem.* **2009**, 635.

[5] M. Wriedt, S. Sellmer, C. Nather, *Dalton Trans.* **2009**, 7975–7984.

[6] C. Näther, J. Greve, *J. Solid State Chem.* **2003**, *176*, 259–265; M. Wriedt, I. Jeß, C. Näther, *Eur. J. Inorg. Chem.* **2009**, 1406–1413; M. Wriedt, S. Sellmer, C. Näther, *Inorg. Chem.* **2009**, *48*, 6896–6903.

[7] C. Näther, J. Greve, I. Jeß, *Chem. Mater.* **2002**, *14*, 4536–4542; J. Greve, I. Jeß, C. Näther, *J. Solid State Chem.* **2003**, *175*, 328–340.

[8] X.-Y. Wang, H.-Y. Wei, Z.-M. Wang, Z.-D. Chen, S. Gao, *Inorg. Chem.* **2005**, *44*, 572–583.

[9] Y. Wang, R. Cao, W. Bi, X. Li, D. Yuan, D. Sun, *Microporous Mesoporous Mater.* **2006**, *91*, 215–220; J. L. Manson, J. G. Lecher, J. Gu, U. Geiser, J. A. Schlueter, R. Henning, X. Wang, A. J. Schultz, H.-J. Koo, M.-H. Whangbod, *Dalton Trans.* **2003**, 2905–2911.

[10] L. T. Yıldırım, O. Atakolb, G. Kavak, *Acta Crystallogr., Sect. E* **2007**, *63*, m2403–m2404.

[11] X.-Y. Wang, L. Gan, S.-W. Zhang, S. Gao, *Inorg. Chem.* **2004**, *43*, 4615–4625.

[12] K. Nakamoto, *Infrared and Raman Spectra of Inorganic and Coordination Compounds*, 4th ed., Wiley, New York, **1986**; A. Abylaikhan, Dissertation, Technische Universität Chemnitz, **2005**; M. Leschke, Dissertation, Technische Universität Chemnitz, **2001**; G. B. Deacon, R. J. Phillips, *Coord. Chem. Rev.* **1980**, *33*, 227–250.

[13] G. Busca, V. Lorenzelli, *Mat. Chem.* **1982**, *7*, 89–126.

[14] A. F. Hollemann, E. Wiberg, *Lehrbuch der Anorganischen Chemie*, 101st ed., de Gruyter, Berlin, New York, **1995**.

[15] G. M. Sheldrick, *Acta Crystallogr., Sect. A* **2008**, *64*, 112–122.

[16] G. A. Bain, J. F. Berry, *J. Chem. Educ.* **2008**, *85*, 532–536.

Received: December 1, 2009
Published Online: March 18, 2010

